Biochimica et Biophysica Acta 1838 (2014) 1738–1751

Contents lists available at ScienceDirect

Biochimica et Biophysica Acta

journal homepage: www.elsevier.com/locate/bbamem

Acidic pH triggers conformational changes at the NH_2-terminal propeptide of the precursor of pulmonary surfactant protein B to form a coiled coil structure

A. Bañares-Hidalgo, J. Pérez-Gil, P. Estrada *

Departamento de Bioquímica y Biología Molecular I, Facultad de Biología, Universidad Complutense, Ciudad Universitaria, 28040 Madrid, Spain

ARTICLE INFO

Article history:
Received 28 January 2014
Received in revised form 19 March 2014
Accepted 24 March 2014
Available online 1 April 2014

Keywords:
Pulmonary surfactant
SP-B
N-terminal propeptide
Coiled coil

ABSTRACT

Pulmonary surfactant protein SP-B is synthesized as a larger precursor, proSP-B. We report that a recombinant form of human SP-B_N forms a coiled coil structure at acidic pH. The protonation of a residue with pK = 4.8 ± 0.06 is the responsible of conformational changes detected by circular dichroism and intrinsic fluorescence emission. Sedimentation velocity analysis showed protein oligomerisation at any pH condition, with an enrichment of the species compatible with a tetramer at acidic pH. Low 2,2,2,-trifluoroethanol concentration promoted β-sheet structures in SP-B_N, which bind Thioflavin T, at acidic pH, whereas it promoted coiled coil structures at neutral pH. The amino acid stretch predicted to form β-sheet parallel association in SP-B_N overlaps with the sequence predicted by several programs to form coiled coil structure. A synthetic peptide (^{60}W-E^{85}) designed from the sequence of the amino acid stretch of SP-B_N predicted to form coiled coil structure showed random coil conformation at neutral pH but concentration-dependent helical structure at acidic pH. Sedimentation velocity analysis of the peptide indicated monomeric state at neutral pH ($s_{20,w}$ = 0.55 S; Mr ~ 3 kDa) and peptide association ($s_{20,w}$ = 1.735 S; Mr = ~ 14 kDa) at acidic pH, with sedimentation equilibrium fitting to a Monomer-Nmer-Mmer model with N = 6 and M = 4 (Mr = 14692 Da). We propose that protein oligomerisation through coiled-coil motifs could then be a general feature in the assembly of functional units in saposin-like proteins in general and in the organization of SP-B in a functional surfactant, in particular.

1. Introduction

The coiled coil motif is formed by two or more α-helices wound around each other in a "superhelix." This structure was first proposed by Crick based on the X-ray fiber diffraction patterns from α-keratins and quill [1]. It is believed to be adopted by 3–5% of all amino acids in proteins [2] and is a ubiquitous protein-folding motif that guides oligomerization in a wide variety of systems, including transcription factors, muscle proteins, intermediate filaments and extracellular fibres. The sequence of all these proteins contain patterns of seven residues (heptads) in which hydrophobic side chains are alternately spaced three and four residues apart. The seven positions of the heptad repeat are assigned **abcdefg** with **a** and **d** occupied by hydrophobic residues [3]. The interaction between two α-helices in a coiled coil involves these hydrophobic residues and the charged residues at the **e** and **g** positions. The simple repeating units of structure in coiled coil, makes them particularly amenable to computer based recognition methods [4]. The prediction of coiled coil from protein sequences was pioneered by Parry who showed that each heptad position has a characteristic residue distribution and proposed to score the coiled coil forming propensity of a sequence by its match to a position-specific scoring matrix derived from these distributions [5].

We are working with the 177 amino acids N-terminal propeptide (SP-B_N) of the precursor of the surfactant protein B (proSP-B) which also contains a C-terminal propeptide, being both propeptides eliminated to form mature surfactant protein B (SP-B). The mature SP-B is necessary to promote the assembly of the pulmonary surfactant, a lipid–protein complex forming surface active films at the air–water interface, thus reducing surface tension to a minimum to stabilize the lung [6]. The N-terminal propeptide of proSP-B is required for targeting, processing and assembly of the hydrophobic mature SP-B into surfactant complexes *in vivo* [7], likely by chaperoning the mature protein [8,9]. We

Abbreviations: MBP, Maltose Binding Protein; MBP-SP-B_N, Fusion MBP-NH_2-terminal propeptide of proSP-B; SP-B_N, NH_2-terminal propeptide of proSP-B; SP-B, Surfactant Protein B; TFE, 2,2,2-trifluoroethanol; ThT, Thioflavin T

* Corresponding author. Tel.: +34 91 3944620; fax: +34 91 3944672.
E-mail addresses: mpestrada@bio.ucm.es, estrada@bbm1.ucm.es (P. Estrada).

http://dx.doi.org/10.1016/j.bbamem.2014.03.016
0005-2736/

have produced a recombinant form of the human N-terminal propeptide by cloning its sequence and expressing it in *E. coli* [10] and we have studied the conditions that favored or hindered its aggregation [11].

ProSP-B is an homologous protein to prosaposin, the precursor protein of four saposins (*sphingolipid activator proteins*) generated through cleavage of the precursor prosaposin [12]. Prosaposin contains four B-type saposin modules (SAPB, the mature saposins A, B, C and D) and two A-type saposin modules (SAPA, within its N- and C-terminal propeptides) whereas proSP-B contains three SAPB modules, in mature SP-B and in both flanking propeptides, plus an additional SAPA module in the N-terminal propeptide (Scheme 1). The position of three intramolecular disulphides in the SAPB modules has been determined experimentally and is strictly conserved, while it has not been established yet, to our knowledge, in any SAPA domain. One of these modules, the SAPB domain of the N-terminal propeptide has been isolated from the bronchoalveolar lavage fluid of rat lung and has shown microbicide properties [13]. This finding has increased the interest for the study of the propeptide and their modules. Saposin B forms a dimer through an antiparallel coiled coil between the two α-helices of their N-terminal segment at acidic pH [14].

In the present work, we have aligned the sequence of the SAPB domain of SP-B_N with the homolog saposin B (PDB accession number 1N69), and generated a monomeric 3D model of SP-B_N with the Phyre2 server [15]. We have determined that certain environmental conditions induce SP-B_N to form β-sheet fibril as surfactant protein C (SP-C) does [16] and that the amino acid patch prone to β-aggregation predicted by PASTA [17] is part of the predicted coiled coil region in the SAPB domain of SP-B_N. Then, we have studied the effect of acid pH on SP-B_N, and, as we detected the formation of a coiled coil structure, several programs have been run to predict the definite sequence forming it. One of them (PROCOIL) [18] has predicted the dimeric character of the coiled coil. Finally, a synthetic peptide encompassing the amino acid stretch of the protein predicted to form coiled coil structure has been synthesized and its secondary structure and hydrodynamic properties have been studied, confirming that this segment could drive oligomerization of the propeptide domain and the whole proSP-B precursor *via* formation of a coiled-coil motif.

2. Materials and methods

2.1. Production and purification of SP-B_N

A pMAL c2x-SP-B_N plasmid construct containing the SP-B_N sequence of human preproSP-B cDNA was used to express the wild-type propeptide in *E. coli* strain UT5600 as a fusion protein with the Maltose Binding Protein (MBP). Purification of the chimera (MBP-SP-B_N) was achieved by affinity chromatography in an amylose resin column. The fusion was cleaved by Factor Xa (Sigma) and purification of the propeptide was carried out by anion exchange chromatography as described [10]. The fractions containing purified SP-B_N in 20 mM Tris–HCl buffer pH 7, 500 mM NaCl were dialyzed towards the buffer needed in subsequent experiments. The propeptide concentration was calculated from its absorbance at 280 nm using $\varepsilon_{280} = 20790\ M^{-1} \cdot cm^{-1}$ [11]. Quantitation of thiols in purified SP-B_N yielded no detectable free cysteines, indicating that all disulphides had been formed (not shown).

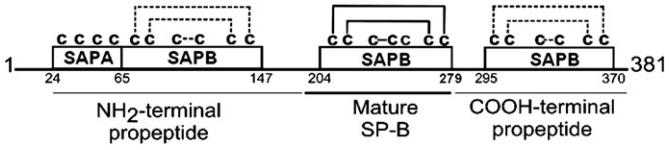

Scheme 1. Structure of human preproSP-B. *Numbers* indicate the amino acid position at the beginning and end of the Saposin A-type like module (SAPA) or the B-type (SAPB). Signal peptide encompasses amino acids 1–23, NH_2-terminal propeptide: 24–200 and mature SP-B: 201–279. Amino acid residues in positions 148–200 correspond to the arm connecting the NH_2-terminal propeptide with mature SP-B. Solid lines between cysteine residues indicate disulphide bonds whereas dashed lines indicate putative disulphide bonds by homology with bonds in saposin modules of preproSaposin [http://www.uniprot.or./uniprot/P07988]. Lighter cysteine in mature SP-B serves to dimerise mature SP-B through interchain disulphide bond. Potential glycosilation site in the NH2-terminal propeptide (N^{129}) is omitted as the protein is produced in bacteria. The second site (N^{311}) in the COOH-terminal propeptide is also omitted.

2.2. Synthesis of peptide ^{60}W–E^{85}

The sequence comprising amino acids 60–85 of SP-B_N was selected from its calculated coiled-coil propensity and a corresponding synthetic peptide was synthesized with the sequence $_{NH2}$WGHVGADDL(Abu)QE(Abu)EDIVHILNKMAKE$_{COOH}$, where the Cys residues in the original sequence have been substituted by Abu (alpha-amino-n-butyric acid), isosteric with Cys, to avoid potential disulphide oligomerization. Synthesis using Fmoc (fluoren-9-ylmethoxycarbonyl) chemistry was carried out at the laboratory of Dr. David Andreu, at Universidad Pompeu Fabra in Barcelona [19]. Once synthesized and liberated from the matrix, the peptide was purified to >95% by HPLC, and its purity was checked by matrix-assisted laser desorption-ionization time-of flight (MALDI-TOF) MS analysis.

2.3. Circular dichroism of SP-B_N and the peptide ^{60}W–E^{85}

Circular dichroism spectra of SP-B_N and peptide ^{60}W–E^{85} were recorded at 25 °C on a Jasco J-715 spectropolarimeter, using thermostated quartz cells of 0.1-cm path length, at 50 nm · min^{-1} (1 s response time) for the far-UV (250–195 nm) spectral range, each spectrum being the accumulation of 5 scans. The spectra were obtained in 200 μL of 5 mM acetate, 5 mM MES, 5 mM Tris buffer (AMT buffer) 150 mM NaCl pH 7 at 0.115 mg mL^{-1} protein unless otherwise stated. Mean residue molar ellipticities [θ] were calculated from the measured ellipticity taking into account the protein concentration, the molecular weight of SP-B_N (19,902 Da, DNA star program) and the number of amino acids per molecule (177). Estimations of the secondary structure content from the CD spectra were performed by using the CDPro suite program and the α-helix and β-sheet contents were calculated using three different methods, CONTIN/LL, SELCON3 and CDSSTR [20], employing their mean value. To record the CD variation with pH the spectra were obtained after shifting the pH of the sample by addition of aliquots of 0.8 N HCl. The pH was assessed in a Mettler-Toledo MP230 pH-meter provided with a microelectrode. Protein concentration was corrected for dilution to process the data. One protein sample was used for each of the pH values during the titration. Samples with 2,2,2,-trifluoroethanol (TFE, Merck) required concentrated protein samples in 5 mM AMT buffer, 150 mM NaCl pH 7 or pH 4.3 that upon dilution with an appropriate amount of commercial TFE reached 0.115 mg mL^{-1}. CD spectra of the synthetic peptide were carried in the same buffer and conditions as above only that 0.05–0.8 mg mL^{-1} was employed.

2.4. Fluorescence of SP-B_N and the peptide ^{60}W–E^{85}

The intrinsic fluorescence emission spectra of SP-B_N were recorded at 25 °C in a SLM-Aminco AB2 spectrofluorimeter using a 1-cm quartz cell with excitation (290 nm), emission slits set at 4 nm and scan speed of 2 nm s^{-1}. The sample contained 0.115 mg mL^{-1} in 5 mM AMT buffer, 150 mM NaCl at the indicated pH, with or without TFE. Fluorescence spectral center of mass (SCM, intensity-weighted average emission wavelength) was calculated according to Eq. (1), being λ the emission wavelength and I(λ) the fluorescence intensity at wavelength λ.

$$SCM = \Sigma\lambda \cdot I(\lambda)/\Sigma I(\lambda) \quad (1)$$

The extrinsic fluorescence emission spectra of 25 μM thioflavin T (ThT, Sigma) with 0.12 mg mL^{-1} protein in 5 mM AMT buffer, 150 mM NaCl pH 4.3 containing 0–40% TFE (v/v) were recorded from 470 nm to 550 nm upon excitation at 450 nm.

The analysis of the pH denaturation data was carried out with Eq. (2):

$$Y_{obs} = \frac{Y_N + a}{1 + \exp\left(\frac{pK - pH}{b}\right)} \quad (2)$$

where Y_{obs} is the observed parameter ($[\theta]^{208}$, the ratio $[\theta]^{220}/[\theta]^{208}$ or SCM) at each pH and Y_N is the parameter value at neutral pH. The midpoint of the curve is the apparent pK of the titrating group and *a* and *b* are constants. It is assumed that both species, protonated and deprotonated, contribute to the fluorescence spectrum. Analysis of the transition curves in the presence of TFE was carried out with Eq. (2) by substituting pK by $D_{1/2}$ and pH by D respectively, being D the TFE concentration and $D_{1/2}$ the midpoint of the curve. Y_{obs} is the parameter value ($[\theta]^{220}/[\theta]^{208}$ or % α-helix content) at each TFE concentration and Y_N is obtained in the absence of TFE.

2.5. Analytical ultracentrifugation studies of SP-B_N and the peptide ^{60}W–E^{85}

Hydrodynamic studies of 0.436 mg mL^{-1} SP-B_N in 5 mM AMT buffer, 150 mM NaCl at pH 7 or 4 were performed at 20 °C and 48,000 rpm in an Optima XL-1 (Beckman-Coulter Inc) analytical ultracentrifuge equipped with UV–visible optics. The partial specific volume $\overline{V}$ of SP-B_N is 0.73 mL g^{-1} estimated from its amino acid composition with the program SEDNTERP, version 1.09 (retrieved from RASMB server) [21]; the solvent density ρ is 1.005 g mL^{-1} and the solvent viscosity η is 1.017 cpoise. Sedimentation velocity of the peptide was carried out using 0.55 mg mL^{-1} (185 μM) peptide concentration in the same buffer at pH 7 or 4.3 at 48,000 rpm and 20 °C. Sedimentation equilibrium of the peptide (same concentration, buffer and pH as in SV analysis) was carried out at 28,000 rpm and 20 °C. The samples were run for 18 h plus an additional 4 h for collecting the scans, and the cells of the ultracentrifuge were scanned at 290 and 298 nm. The theoretical absorption molar coefficient at 280 nm of the synthetic peptide was predicted by ProtParam tool of the ExPASy web site [22] to be 5500 M^{-1} cm^{-1}, assuming that the peptide holds Cys residues instead of Abu. Its theoretical pI is 4.72 and its instability index is 72.08, which classifies the peptide as unstable. The partial specific volume of the peptide has been calculated as 0.73 mL g^{-1} considering Cys instead of Abu and the measured solvent density is 1.007 g mL^{-1}. The absorption molar coefficient at 290 nm was calculated multiplying its value at 280 nm by the absorbance ratio at both wavelengths and was $\varepsilon_{290} = 1$ $(mg\ mL)^{-1}$ cm^{-1}. The SE analysis data were analyzed by the HeteroAnalysis software 1.1.44 of Cole [23].

2.6. Structure prediction analysis on SP-B_N and on the peptide ^{60}W–E^{85}

The sequence of SP-B_N was subjected to secondary structure prediction analysis, using the GOR (acronym of Garnier/Osguthorpe/Robson) program (V.2, 1998) [24]. The program PSIPRED V2.6 [25] was also employed. Coiled coil propensities were scored with the program COILS2 (version 2.2), which is an extension of COILS [26] and weights the core residues **a** and **d** 2.5 times higher than the other residues, thus placing increased emphasis on the continuity of the hydrophobic repeat pattern [27]. Other programs employed to predict coiled coil structures were MATCHER [28], PEPCOIL, an application written by Bleasby on the original of Rice (EGCG 1991) [29] based on the Lupas work [26], and MULTICOILS [30]. The prediction of the predicted coiled coil sequences to form dimeric or trimeric associations was carried out with PROCOIL [18] and the computational method for predicting protein aggregation was PASTA [17]. The secondary structure of the peptide was predicted by AGADIR [31]. The model for the tertiary structure of the SAPB domain (^{65}A–S^{145}) of monomeric SP-B_N was built by the Phyre2 server [15], based on the structure of saposin B obtained by its diffraction data collected at pH 5 [14].

3. Results

3.1. Effect of acidic pH on the secondary and tertiary structure of SP-B_N

The effect that acidification of the medium has on the secondary structure of SP-B_N was analyzed by means of far-UV CD spectroscopy, as illustrated in Fig. 1. Fig. 1A shows how at middle acidic pH, 4.1, 4.3 and 4.6, the minima of the CD spectra became inverted, being the ellipticity more negative at 220 nm than at 208 nm. Further acidification to pH 2.9 reverted again the relative value of ellipticity minima. In the plot of the ellipticities $[\theta]^{220}/[\theta]^{208}$ ratio *vs* pH in Fig. 1B, the initial value evolves from 0.87 to 1.1 following a pH shift from 7 to 4.1 and decreases again upon further acidification. A ratio $[\theta]^{220}/[\theta]^{208} > 1$ is a well known index for coiled coil formation [32], suggesting that SP-B_N may form a coiled coil structure around pH 4. A biphasic transition is observed for the changes in ellipticity in the pH range of 7–4.1 and the fitting of the data to Eq. (2) gives an apparent $pK = 4.8 \pm 0.06$. This value points to the potential protonation of a carboxyl residue as the responsible for the protein conformational change from α-helix-rich to coiled coil structure, although a histidine residue with low pK cannot be totally discarded. At lower pH values, the protonation of a second residue could reverse the coiled coil structure to regain the α-helix-rich structure. All carboxyl residues would be likely protonated around pH 3, unless they form salt bridges with histidines as T4 lysozyme does (pK ~ 0.5) [33]. Therefore, the maximal positive charge the protein holds at pH 2.9 would promote its α-helicity, a behavior also shown by other proteins such as α-lactalbumin [34].

Seeking for changes in the SP-B_N tertiary structure upon pH acidification, we analyzed the intrinsic fluorescence emission spectra of the protein (Fig. 1D). An isofluorescent point (IP) at ~300 nm suggests that, regarding the trp residues environment, only two species are present. The decrease in the fluorescence intensity as the pH drops suggests fluorescence quenching of trp residues by polarizable groups in their vicinity, either glutamic or aspartic acids, which are converted upon protonation in moderate quenchers, or histidine, which is converted upon protonation into a strong quencher [35]. The variation with pH of the spectral center of mass (SCM), an index of the average energy value of the spectrum, shown in Fig. 1E, is characteristic of an apparent cooperative process. The data were analyzed assuming a two-state conformational change upon protonation of an amino acid residue and their fitting to Eq. (2) gave an apparent $pK = 4.74 \pm 0.15$. As this pK value is practically coincident with the one obtained by CD analysis, it follows that they may belong to the same residue. The plateau observed for the SCM above pH 5.6 and below pH 4 appears to correspond to stable forms of the protein regarding its tertiary structure. As the parallelism between secondary and tertiary structure is only seen from neutral to pH ~ 4 excluding the lowest pHs, a typical two-state conformational transition taking place in the whole SP-B_N upon acidification can be ruled out.

3.2. Effect of protein concentration on SP-B_N secondary structure

As a ratio $[\theta]^{220}/[\theta]^{208} > 1$ around pH 4 in Fig. 1B suggested that SP-B_N could form a coiled coil structure, we have determined whether there was an effect of the protein concentration on the CD signal. Fig. 1C represents $[\theta]^{208}$ vs SP-B_N concentration. No concentration dependence was observed at pH 7, a result expected if intermolecular associations among protein molecules are absent. At pH 4, however, the ellipticity shows dependence on protein concentration, which is expected if intermolecular associations take place, confirming the potential coiled coil formation at this pH. As the protein concentration increases, the $n \leftrightarrow 2n$ equilibrium would shift towards the formation of coiled coil 2n, which would increase the α-helical content of the protein as it has been observed for other proteins [36], independently of *n* being a monomer or a higher order oligomer.

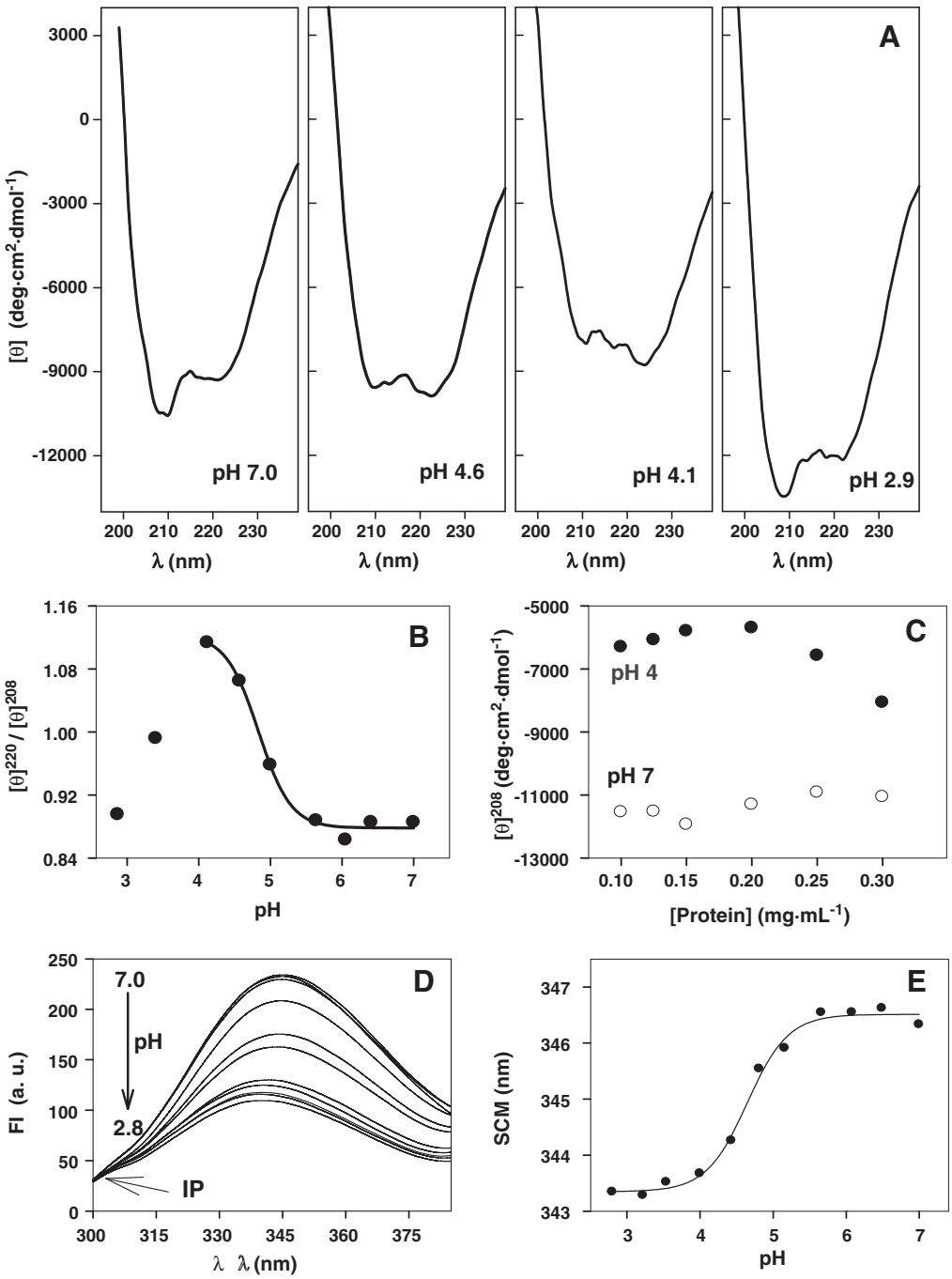

Fig. 1. Effect of acid pH on SP-B_N secondary and tertiary structure. A) A selection of far-UV CD spectra of the protein in the pH range of 2.9–7. B) Variation of the molar ellipticities ratio at 220 and 208 nm with pH. The curve through the data is a fit to Eq. (2). C) Effect of the protein concentration (0.1–0.3 mg mL^{-1}) on the $[\theta]^{208}$ at pH 7 (void circles) and pH 4 (filled circles). D) Fluorescence intensity emission spectra of the protein in the pH range of 2.8–7. IP is isofluorescent point. E) Variation of the SCM calculated (300–385 nm) through Eq. (1) with pH (filled circles). The curve through the data is a fit to Eq. (2).

3.3. Effect of 2,2,2-trifluoroethanol on SP-B_N secondary structure

Further evidence that the intermolecular interaction around pH 4.3 is a consequence of coiled coil formation was obtained from TFE titration (Fig. 2). The effect of TFE on the CD spectra is depicted in Fig. 2A, where three distinct different shapes can be distinguished, as well as a possible intermediate or transition form. In 50–70% TFE (v/v), the spectra of SP-B_N show the typical $\alpha + \beta$ conformation shape (minimum at 208 nm deeper than that at 220 nm) whereas in the absence of the solvent and in the presence of 40% TFE, the shape is just the opposite suggesting coiled coil structures. With 10–20% TFE the spectra display a single minimum at around 230 nm, typical of proteins suffering β-sheet aggregation in amyloid-like structures as described for other proteins either with low TFE or promoted by pH changes [37]. With 30% TFE, the spectrum shows two minima at 228 nm and 209 nm. It may correspond to a transition form from β-sheet amyloid-like aggregate to α-helix structure or to a distorted α-helix (regular α-helix with reduced amplitudes and shifted wavelengths) [38]. In agreement with the existence of the three mentioned conformers, two isodichroic points (IP) are observed in Fig. 2A. In the IP at 199 nm (encircled), all spectra cross-over except those obtained with 10 and 20% TFE, suggesting a transition from coiled coil to α-helix-rich structures. The second IP

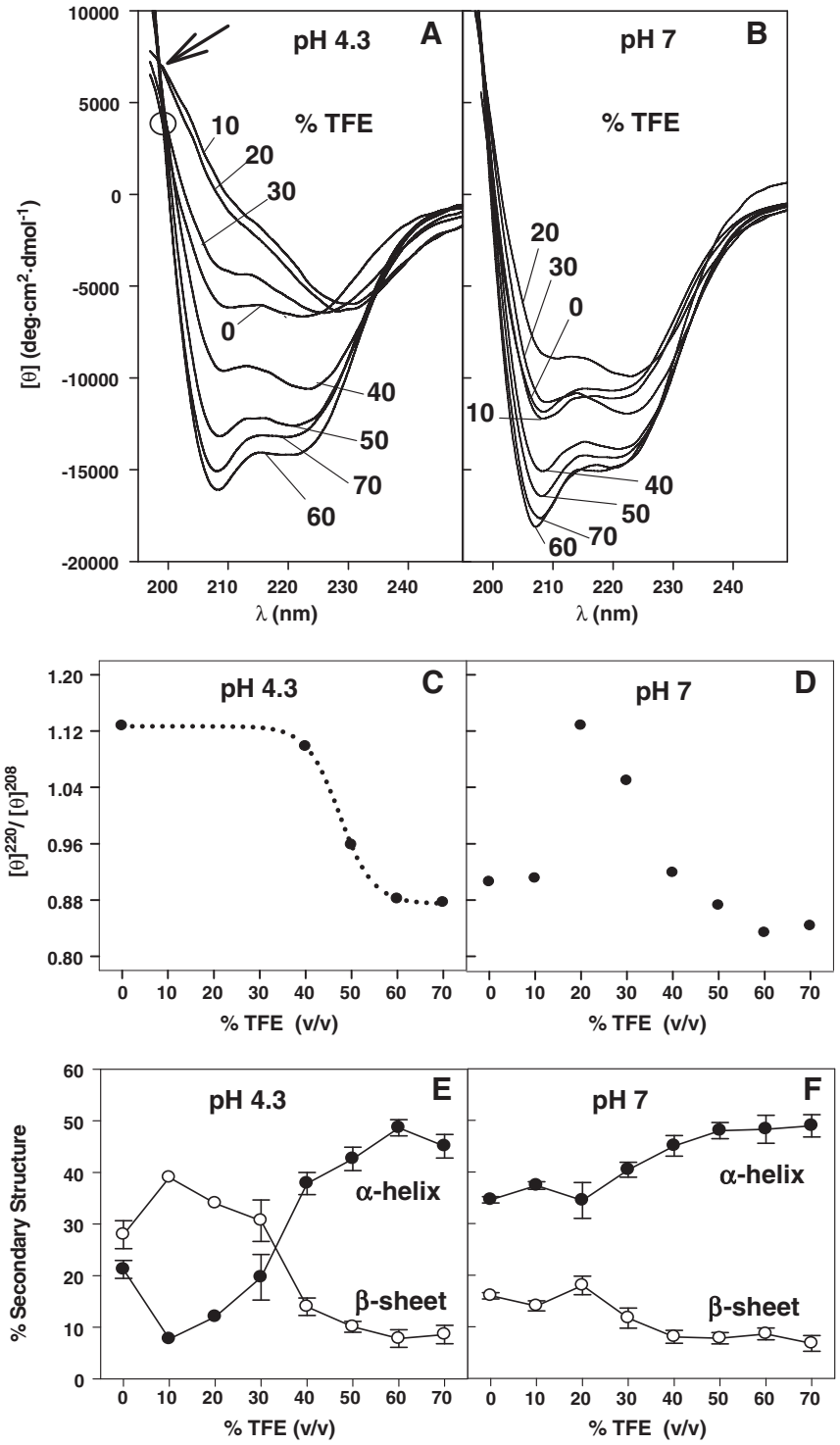

Fig. 2. Effect of TFE on the secondary structure of SP-B_N. A) Far-UV CD spectra of SP-B_N in 5 mM AMT buffer, 150 mM NaCl pH 4.3 containing 0 to 70% (v/v) TFE. B) Same as in A except that the pH was 7. C) Variation of $[\theta]^{220}/[\theta]^{208}$ with TFE concentration at pH 4.3. The dotted line is a fit of the data in plot to Eq. (2). The ratio values obtained with 10, 20 and 30% (v/v) TFE were: −3.53, −35.76 and 1.47 respectively and have been excluded both from the plot and from the fit. D) Same as in C at pH 7. E) Variation of the α-helix (filled circles) and β-sheet (void circles) percent content with TFE at pH 4.3. F) Same as in E at pH 7.

is also observed at 199 nm (arrowed, displaying twice the ellipticity of the first one) where all spectra intersect excepting those corresponding to the protein plus 30% TFE and to the protein in the absence of TFE. This second IP may correspond to a structural change from the transition form (or the distorted α-helix if it is the case) to α-helix-rich structure. One pertinent example of protein showing more than one two-state structural transitions is the E4orf6 adenovirus protein, which adopts several conformations following exposure to TFE [39].

To check the disruption by TFE of the coiled coil at pH 4.3, Fig. 2C plots the $[\theta]^{220}/[\theta]^{208}$ ratio vs TFE concentration. This ratio, above 1 in the absence of TFE, decreases to ~ 0.88 following a sigmoid curve above 40% TFE. As the spectra of the protein in exposed to 10, 20 or 30% TFE did not correspond to an α-helical conformation, the corresponding $[\theta]^{220}/[\theta]^{208}$ ratios (−3.53, −35.76 and 1.47 respectively) have not been included into the plot. Therefore, it seems that SP-B_N suffers several transitions at pH 4.3 from coiled coil (in the absence of TFE)

to amyloid-like aggregates (10–20% TFE), to a transition form (~30% TFE) and to α-helix rich conformation (above 40% TFE). The transition point from coiled coil (at 40% TFE) to α-helix rich structure at higher TFE proportions in Fig. 2C cannot be determined unless we add a data not belonging to the transition (at 0% TFE). This additional point in the plot allows for a good definition of the plateau and the subsequent fit to Eq. (2), obtaining an apparent transition point of 47.4 ± 0.12% (v/v) TFE. The results obtained in the presence of TFE agree with previous reports regarding its role as disturber of intermolecular associations at high concentration whereas at low concentration promotes the formation of quaternary structure [40]. A model has been proposed to explain this effect. At low TFE, where the TFE clusters are not fully developed or stabilized, TFE draws water away from the surface of proteins. As the TFE concentration increases and the cluster size of the fluoroalcohol becomes larger, the clusters may associate directly with hydrophobic side chains decreasing the side-chain conformational entropy; that decrease may be important in the formation of α-helices [41]. The clustering of alcohol molecules is considered to be an important factor to promote the effects of the alcohol. The clusters reduce the polarity around the proteins, and therefore strengthen the hydrogen bonds, more effectively than dispersed alcohol molecules do [42].

The effect of TFE addition on the CD spectrum of SP-B_N at pH 7 is depicted in Fig. 2B. The relative values of the minima in the absence of TFE (more pronounced at 220 nm than at 208 nm) are inverted in the presence of 20 or 30% TFE. Accordingly, the $[\theta]^{220}/[\theta]^{208}$ ratio is above 1 at 20–30% TFE, suggesting that these TFE concentrations, which promoted amyloid-like structure at pH 4.3, may promote coiled-coil structure at pH 7. The secondary structure contents *vs* TFE concentration at pH 4.3 and pH 7 are plotted in Fig. 2E and F, respectively. The α-helical content of the protein in the presence of TFE (21.2 ± 1.7%) at acidic pH, decreases sharply at 10% TFE, to increase with TFE concentration thereafter up to ~50% α-helix at 60–70% TFE, whereas the initial β-sheet content (27.9 ± 2.7%) follows the reverse way. The initial turn (21.3 ± 1.7%) and random coil (28 ± 1.6%) content suffer practically no changes upon TFE addition (not shown). At pH 7, the initial α-helix and β-sheet content suffer small variations al low TFE to increase and decrease respectively above 30% TFE (Fig. 2F). The initial turn (21.4 ± 1.2%) and random coil (28.8 ± 0.9%) content at neutral pH remain practically unchanged as the TFE concentration is increased (not shown).

3.4. Extrinsic and intrinsic fluorescence studies with TFE

Extrinsic fluorescence was measured with the probe Thioflavin T (ThT), a dye composed of benzothiazole and benzaminic rings freely rotating around a shared C–C bond. This rotation is hindered upon binding of ThT to amyloid aggregates, resulting in fluorescence emission of ThT upon excitation around 440 nm [43]. A maximum at 482 nm in aqueous solutions is indicative of the presence of amyloid [44] although the maximum may be slightly displaced in the presence of alcohols. It has been observed that certain TFE concentrations promote protein aggregation and that the aggregates reorganize themselves into amyloid-like fibrils [45] and thus, we have employed ThT to reveal the presence of SP-B_N aggregates with a relatively ordered organization at pH 4.3 in the presence of TFE (Fig. 3A). ThT fluorescence increased notably at 20–30% TFE to decrease at higher TFE proportions. The dependence of the ThT emission at 483 nm on TFE concentration is depicted in the inset of Fig. 3A. The fluorescence emission by ThT bound to the protein confirms the formation of amyloid-like β-sheet aggregates by SP-B_N at 20–30% TFE and, to a lesser extent, at 10% TFE. Whether these ThT-sensitive SP-B_N aggregates adopt or not amyloid-like fibrillar morphologies must still to be explored, *i.e.* by electron microscopy, something which is beyond the scope of the present work. The detection of aggregates at 30% TFE also confirms that this TFE concentration is the responsible for the transition from aggregates to α-helix rich structures (see Fig. 2A).

The intrinsic fluorescence of SP-B_N was also monitored in the presence of TFE at acidic pH, to check whether the changes observed in protein fluorescence emission hold parallelism with the observed in protein secondary structure under the same conditions. The emission spectra recorded upon excitation at 290 nm and compared in Fig. 3B show an increase in the fluorescence intensity as the TFE concentration increases, indicating that the emission of trp residues is becoming less quenched. The variation of SCM with the TFE concentration (Fig. 3B, inset) follows a sigmoid curve indicative of a two-state transition in the protein tertiary structure, instead of the several transitions observed in the secondary structure (see Fig. 2A). The fitting of the data to Eq. (2) gave a midpoint at 32.7 ± 2.3% TFE, a lower value than that obtained in the CD experiments (47.4 ± 0.12% TFE, Fig. 2C) when the results concerning 10, 20 and 30% TFE were omitted in the fit. It therefore appears that the conformational change in tertiary structure precedes the change observed in secondary structure from coiled coil to α-helix rich structure (upon changing from 40 to 70% TFE), independently of other changes in secondary structure observed at lower TFE.

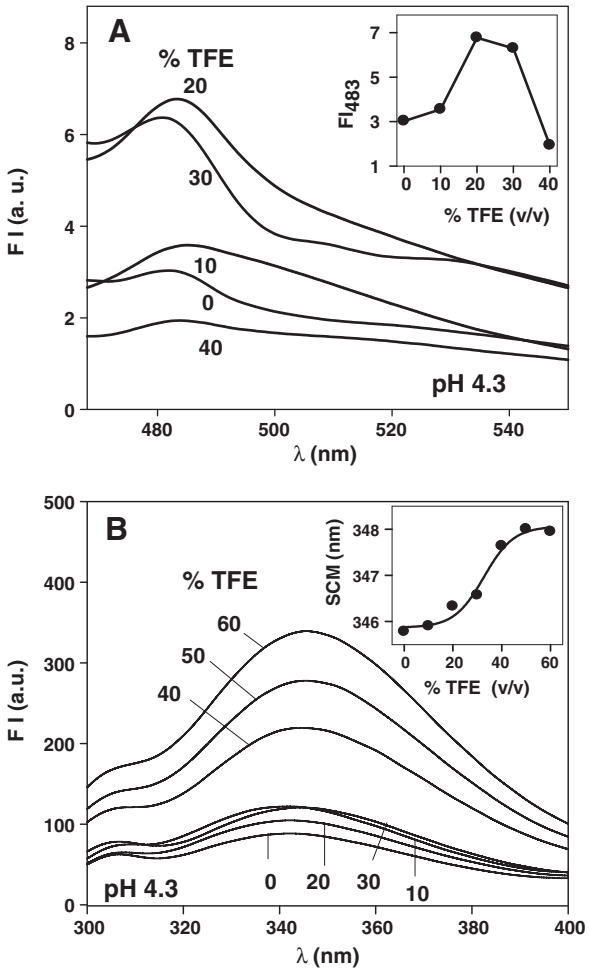

Fig. 3. Extrinsic and intrinsic fluorescence emission in the presence of TFE at acid pH. A) Fluorescence emission spectra of ThT in 5 mM AMT buffer, 150 mM NaCl at pH 4.3 with SP-B_N and 0–40% TFE (v/v) upon excitation at 450 nm. Inset: Dependence of the fluorescence intensity at the maximum wavelength (483 nm) on TFE concentration. B) Effect of TFE on the tertiary structure of SP-B_N. Emission spectra were obtained in the presence of 0–60% (v/v) TFE at pH 4.3. Inset: Variation of the SCM with TFE concentration. The line is a fit of data in plot to Eq. (2).

3.5. Hydrodynamic studies on SP-B_N

To get insight into the oligomeric state of the protein and to approach the molecular mass of the species, a sedimentation velocity analysis of SP-B_N at pH 7 and pH 4.3 was carried out. The sedimentation velocity distributions c(s) of SP-B_N are plotted in Fig. 4 and the parameters: s (raw

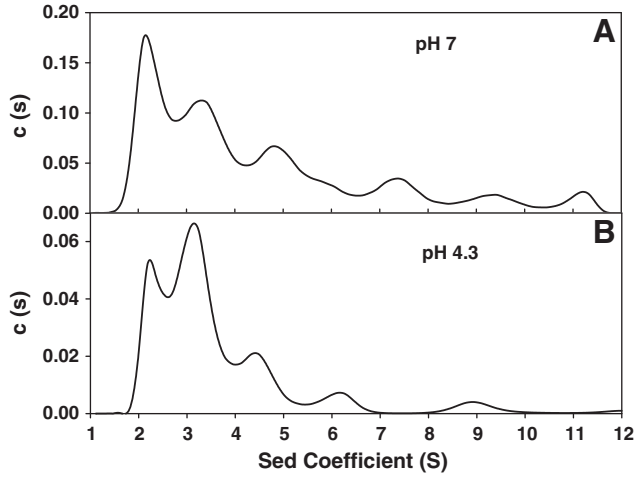

Fig. 4. Sedimentation velocity determination of SP-B_N. A) Sedimentation coefficient distribution at 20 °C and 48,000 rpm of the propeptide (0.436 mg mL^{-1}) in 5 mM AMT buffer, 150 mM NaCl pH 7. B) Same conditions as in A except that the pH was 4.3.

sedimentation coefficient), $s_{20,w}$ (sedimentation coefficient at 20 °C in water, standard conditions) and the frictional ratio (f/f0) are summarized in Table 1. At pH 7, three main species account for 80% of the protein preparation (Fig. 4A). A peak enclosing 30.4% of the mass, with a Stokes Radius of 3.6 nm and $s_{20,w} = 2.35$ S (M ~ 35.6 kDa) is compatible with a dimer of SP-B_N with best frictional ratio f/f0 = 1.77, which indicates that the species is somewhat elongated: a/b (oblate) = 10.11; a/b (prolate) = 9.02. Another peak (30.6% mass) and $s_{20,w} = 3.51$ S (M ~ 65 kDa) is compatible with the protein tetramer whereas 18.5% of the SP-B_N mass was seen as a peak $s_{20,w} = 5.04$ S, M ~ 112 kDa which could be compatible with a hexamer. The remaining of the detected protein includes several additional species with s = 7.46 S, s = 9.58 S, etc. When the sedimentation experiment was carried out at pH 4.3, the corresponding sedimentation profile in Fig. 4B shows that the predominant species, accounting for 50.5% of the mass, shows $s_{20,w} = 3.31$ S, that is, the mixture has been enriched in the species compatible with the tetramer whereas the species compatible with the dimer ($s_{20,w} = 2.35$ S) accounts for 23.5% of the protein mass. The 16.1% of the remaining mass is seen in a peak with $s_{20,w} = 4.65$ S compatible with a hexamer. The enrichment of the mixture in the tetramer at pH 4.3 together with the coiled coil structure deduced from the CD experiments at acid pH (discussed above) point to the coiled coil as a structural motif driving the association of two SP-B_N dimers after the protonation of amino acid residues.

3.6. Prediction studies on SP-B_N structure

The sequence of SP-B_N subjected to secondary structure prediction analysis with GOR and PSIPRED (Fig. 5, upper panel) showed propensity to adopt 34% and 43% α-helix respectively (discarding helix patches with less than 7 amino acids) which is the same and slightly higher respectively than that found in SP-B_N according to CD analysis. The CD data (with and without TFE) pointed to the existence in SP-B_N of a coiled coil structure at acidic pH (see Figs. 2C and 1 B), whereas sedimentation velocity analysis (Fig. 4) established the tendency of the propeptide to oligomerize. It is known that the coiled coil structure in proteins is formed by two or more α-helices wound around each other in a "superhelical" bundle, which guides many oligomerization processes. The sequence of all these proteins contain patterns of seven residues (heptads) in which hydrophobic side chains are alternately spaced three and four residues apart. The seven positions of the heptad repeat are often assigned **abcdefg** with **a** and **d** as the hydrophobic sites [3]. The interaction between two α-helices in a coiled coil involves these hydrophobic, as well as the predominantly charged residues at the **e** and **g** positions. We employed several programs to detect and to compare the sequences in SP-B_N with respect to their propensity to form coiled coil, and the results are summarized in Fig. 5 (bottom panel). COILS2 predicts a single unbroken register, that is, 3 heptads **abcdefg** (probability = 0.117) encompassing residues ^{65}A–E^{85} of the SAPB domain. A^{65} is the last residue in the propeptide SAPA domain but its inclusion into the coiled coil prediction makes it a borderline residue between SAPA and SAPB domains. MULTICOILS predicts 2 heptads encompassing residues ^{76}V–Q^{89} with low probability, whereas PEPCOIL predicts, with high probability (0.825), the propensity to form coiled coil of 14 residues (^{73}E–A^{86}) without defining the position occupied by the residues in the heptad. The longer sequence predicted to form coiled coil was provided by MATCHER (^{65}A–L^{103}), which identified a broken register, that is, 3 heptads (**abcdefg**), 2 stutters (abcd) and twice a stutter plus a skip (abcde). Stutters are discontinuities in the heptad inserting 4 residues, which do not disrupt a continuous coiled coil but introduce a local distortion of the coiled coil geometry (phase shifts). Stammers means the insertion of 3 residues whereas skips means insertion of one residue (shifting the phase by one residue) being formally equivalent to two consecutive stutters. The consequence of the existence of discontinuities (phase shifts) is the variation of the pitch and the radius of the superhelix along the length of the structure [46].

It is also possible to predict whether the coiled coil in protein sequences with propensity to form superhelix is prone to form a dimeric or a trimeric assembly using the PROCOIL algorithm, which plots the contribution of each residue of the chosen sequence to the discriminant function. The absolute discriminant value obtained was dependent on the sequence length and the position of the residue in the heptad, and the more negative this value is for a residue the more this residue contributes to an oligomerization tendency towards the dimer. Positive values would point to a trimer and values close to cero would indicate borderline cases. The search by PROCOIL of dimer or trimer formation in the SP-B_N sequences supposedly forming coiled coil (see Fig. 5, bottom panel) predicted always dimer formation. We have chosen the oligomerization profile of one of these searches, the relative to the sequence ^{65}A–E^{85} (COILS2, 3 heptads) which gave a discriminant function value of −0.75 (Fig. 6, left upper panel). In other sequences such as ^{65}A–L^{103} (MATCHER, 3 heptads plus stutters), the value was −1.14, whereas the sequence ^{76}V–Q^{89} (MULTICOILS, 2 heptads) exhibit the lowest discriminant function (−1.26). All those values indicate, in any case, a strong propensity of the mentioned sequences to dimerize since the standard example (GCN4 yeast protein, PROCOIL handbook) shows a discriminant value of only −0.015, and it is a well known example of dimer formation [47]. Disregarding the program employed, all the sequence patches of SP-B_N predicted to form coiled coil structure lie in the SAPB domain. We have depicted the helical wheel representation

Table 1
The experimental (raw) sedimentation coefficient at the indicated conditions is s and $s_{20,w}$ is the sedimentation coefficient in standard conditions (20 °C, water) expressed in Svedberg (S). f/f0 is the translational frictional ratio of SP-B_N to a perfect sphere.

Sedimentation velocity parameters of SP-B_N			
	Parameters		
Conditions	s (S)	$s_{20,w}$ (S)	f/f0
pH 7	2.27 ± 0.13 3.39 ± 0.24 4.87 ± 0.17	2.35 ± 0.13 3.51 ± 0.23 5.04 ± 0.17	1.77
pH 4.3	2.27 ± 0.19 3.20 ± 0.34 4.49 ± 0.36	2.35 ± 0.19 3.31 ± 0.35 4.65 ± 0.37	1.77

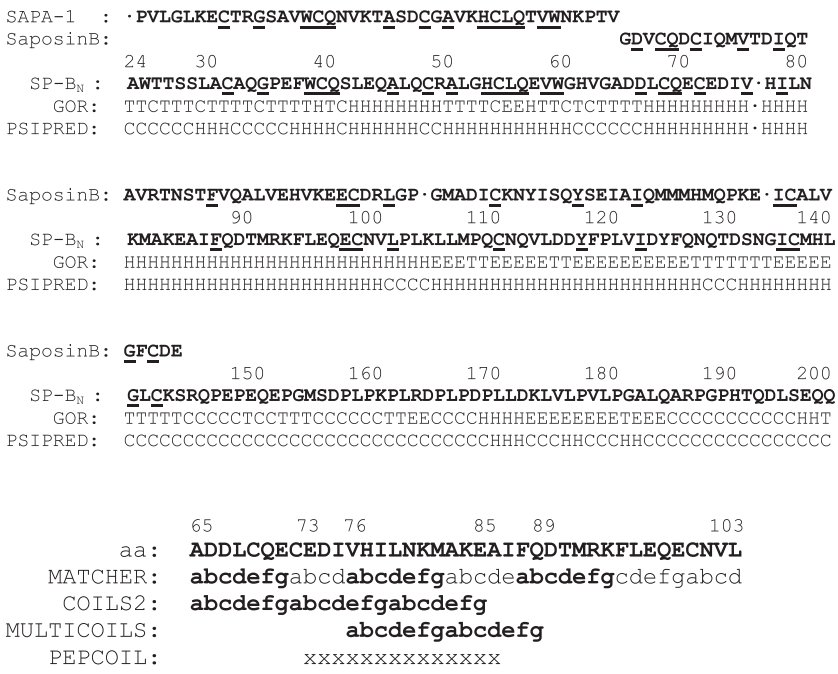

Fig. 5. SP-B_N primary structure and predictions of secondary structure and of coiled coil formation. Upper panel: Sequence alignment of SP-B_N with Saposin B and SAPA-1 domain of prosaposin sequences. α-helix (H), extended strand (E), turn (T) and random coil (C) are indicated below the amino acid sequence of SP-B_N according to the prediction programs. The first 23 aa of preproSP-B (signal) are omitted. Numbers are allusive only to SP-B_N sequence. Conserved residues (30%) between SAPB domain (^{66}D–S^{145}) of SP-B_N and saposin B are underlined. Conserved residues (34%) between SAPA domain (^{25}W–A^{65}) of SP-B_N and SAPA-1 domain of prosaposin (^{18}P–V^{58} in prosaposin sequence) are also underlined. ^{146}R–Q^{200} is the arm connecting the propeptide SP-B_N with mature SP-B. Bottom panel: Prediction frames of coiled coil formation by SP-B_N according to several programs. The predicted frames are shown below the corresponding sequence: ^{65}A–L^{103} (MATCHER), ^{65}A–E^{85} (COILS2) and ^{76}V–Q^{89} (MULTICOILS). Heptads are indicated in bold whereas stutters, stammers and skips are indicated in regular letters. PEPCOIL (^{73}E–A^{86}) did not predict the heptad position of residues and they were named as x.

of coiled coil formation of one of the sequences predicted: the three heptads (COILS2, ^{65}A–E^{85} sequence) in Fig. 6 (medium panel). We have assumed an antiparallel coiled coil structure based on several indications. First, dimeric saposin B at pH 5.8 shows antiparallel coiled coil between the two α-helices of their N-terminal segment [14] and since the SAPB domain of SP-B_N exhibit sequence homology with saposin B (see Fig. 5, upper panel), it is reasonable to assume that there must be structural similarities. Second, Ala in core positions (**a** or **d′**) has been proposed to contribute to antiparallel specificity in coiled coils [48]. Third, Ile residues in positions **d–d′** cannot be accommodated in parallel coiled coils [49] since β-branched residues confer a preference for trimers or tetramers over dimers when located at the **d** position of parallel oligomers [50]. In addition, charged groups in positions **e** and **g** can determine the polarity of the two chains. If, on average, the charges in **e** and **g** are opposite, then the two chains tend to be parallel. Other arrangements can make the chains antiparallel [51]. If we inspect the wheel diagram of ^{65}A–E^{85} in Fig. 6 (medium panel), we see that A^{65} occupies position **a** and I^{78} occupies position **d**, thus pointing to antiparallel coiled coil formation. The fact that there are no groups with opposite charge in **e** and **g**, increases even more the probability for antiparallel coiled coil. Assuming the antiparallel coiled coil, the existence of negatively charged residues (Glu) at **g** and **g′** positions would create electrostatic repulsion at pH 7 hindering the coiled coil stability. The protonation of Glu residues (E^{71} and E^{85}) at acid pH would eliminate the charge repulsion and would stabilize the coiled coil.

There is sequence homology between saposin B and the SAPB domain of SP-B_N [12] and it is known that saposin B forms a dimer at pH 5.8 through an antiparallel coiled coil between the two α-helices of their N-terminal [14]. The 3D structure of the SAPB domain (^{65}A–S^{145}) has been predicted with the Phyre2 server [15] through template-based homology modelling. The result is depicted in Fig. 6 (right upper panel) as a ribbon diagram with four helices. The sequence with propensity to form coiled coil (^{65}A–E^{85}, COILS) would be located in helix 1. The transition to helix 2 holds the residue I^{87} and the transition to helix 3 holds P^{104} whereas a loop encompassing ^{129}N–D^{132} residues gives way to the small helix 4. No 3D structure prediction could be obtained for the SAPA domain due to the lack of a template amongst the 180 SAPA domains defined in 121 proteins in the SMART's nrdb database.

Finally, the sequence ^{75}I–N^{80} located in the putative helix 1 of SAPB domain, is predicted by PASTA to form parallel β-aggregation with the ^{75}I–N^{80} sequence of another protein molecule (Fig. 6, bottom panel, energy = −7.44). Since SP-B_N suffers β-aggregation at pH 4.3 and 10–20% (v/v) TFE, as evidenced by CD and ThT fluorescence analysis, we propose that the segment encompassed by ^{75}I–N^{80} residues would organize the observed β-aggregation. The prediction of different structures in overlapped sequences could indicate that the corresponding patch of amino acid residues in the SAPB domain exhibits plasticity and, depending on environmental conditions, might adopt α-helix or β-sheet structures giving rise to coiled coil structure or facilitating beta-aggregation respectively.

3.7. Secondary structure of synthetic peptide ^{60}W–E^{85}

To check whether the SP-B_N sequence prone to form coiled coil associates once isolated from the protein context, a peptide encompassing the sequence ^{65}A–E^{85} was designed and synthesized. The N-terminal end of the peptide has been extended 5 residues longer (bold letter, see sequence below) than the sequence predicted to form the coil in order to include a Trp residue for future intrinsic fluorescence studies. To prevent formation of undesirable disulphide bridges, the two Cys residues in the wild-type sequence were substituted by α-aminobutyric acid (Abu), an amino acid analogue isosteric with Cys (B), which showed no constrained effect on other peptide structures [52] and did not destabilized them as did the substitution by other residues such as Ala [53].

^{60}**WGHVG**ADDLBQEBEDIVHILNKMAKE^{85}

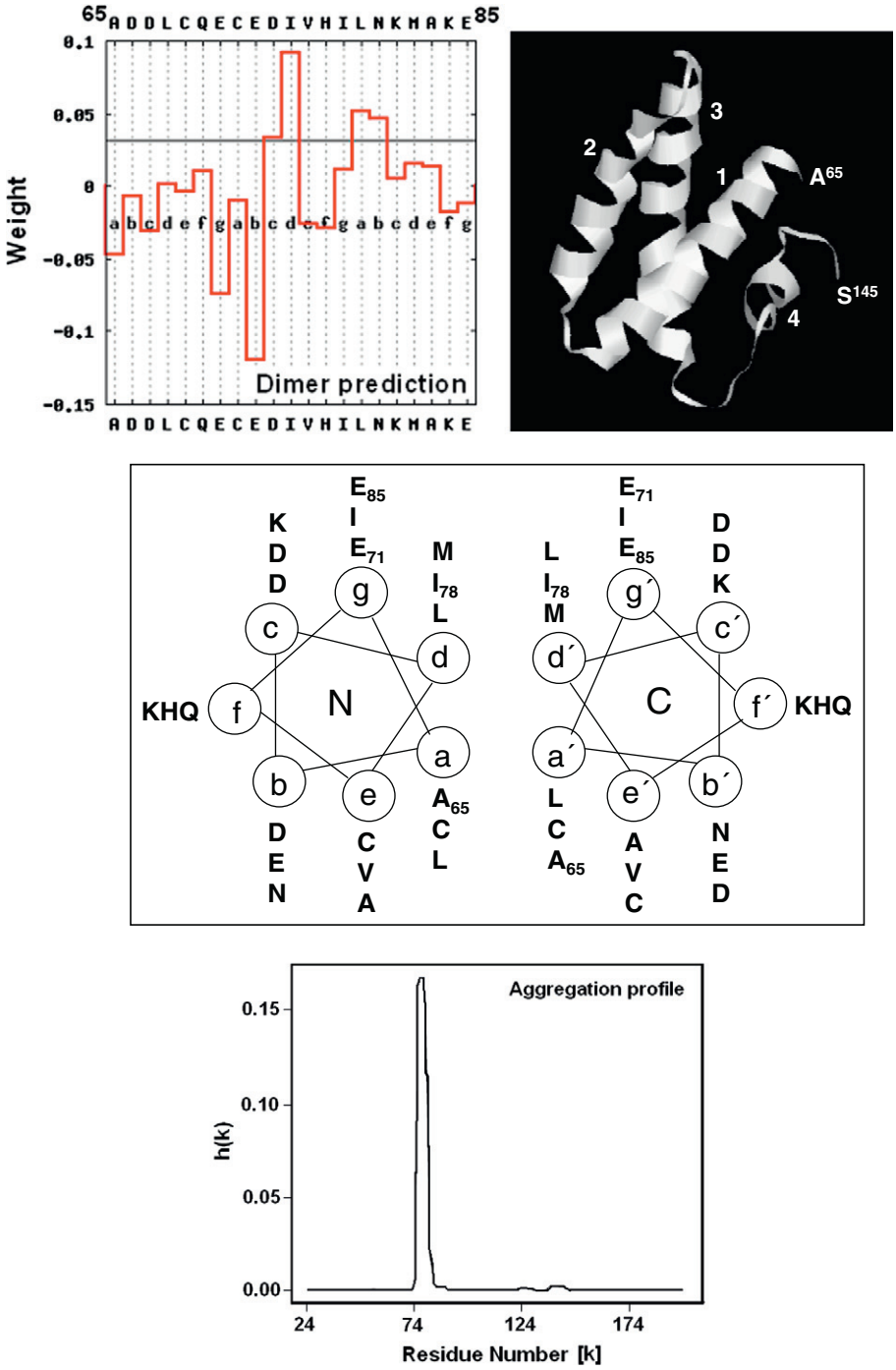

Fig. 6. Prediction of SP-B_N dimer formation, β-aggregation propension and tertiary structure of its SAPB domain. Antiparallel helical wheel representation of the sequence predicted to form coiled coil. Left upper panel: Dimerisation prediction profile of ^{65}A–E^{85} with PROCOIL according to the coiled coil prediction by COILS2 (three heptads). The discriminant function value obtained as the area above the grey baseline minus the area below the grey baseline is −0.74. Right upper panel: Ribbon diagram of the predicted tertiary structure of the SAPB domain (^{65}A–S^{145}) of SP-B_N. Medium panel: Helical-wheel representation of residues ^{65}A–E^{85} of the SP-B_N sequence. Relative amino acids position on the α-helical wheel (3 heptads) was according to COILS2 and the depicted coiled coil is antiparallel. The view is from the N- and C-terminus respectively as indicated looking down the α-helical axes, that is, the direction of the chain is indicated by whether the N- or C-terminus is out of the page. Heptad repeat positions are circled and labelled **a-g** and **a′-g′**. Bottom panel: Aggregation profile of SP-B_N by PASTA algorithm.

The secondary structure of the peptide has been analyzed by far-UV CD in the presence or in the absence of TFE, as summarized in Fig. 7. The CD spectra in the absence of TFE are shown in Fig. 7A within a peptide concentration range of 0.05 mg mL^{-1} (17 μM) to 0.85 mg mL^{-1} (287 μM). The spectrum obtained at the lowest peptide concentration displays a minimum of ellipticity at 199 nm (dotted line), typical of a random coil, which agrees with only 0.81% of α-helix predicted by AGADIR for the monomeric peptide at 25 °C, pH 7 and 0.15 M ionic strength. The lack of dependence of the ellipticity at 220 nm on the peptide concentration (inset) indicates that no oligomerization or aggregation processes takes place at this pH. This result was not unexpected since the substitution by Abu of ^{69}C and ^{73}C residues, which presumably form disulphide bridges with other Cys in the protein context (Scheme 1), must reduce the peptide association stability compared with the whole protein molecule. Other peptides in literature showed similar behavior. Peptides designed from segments predicted to form

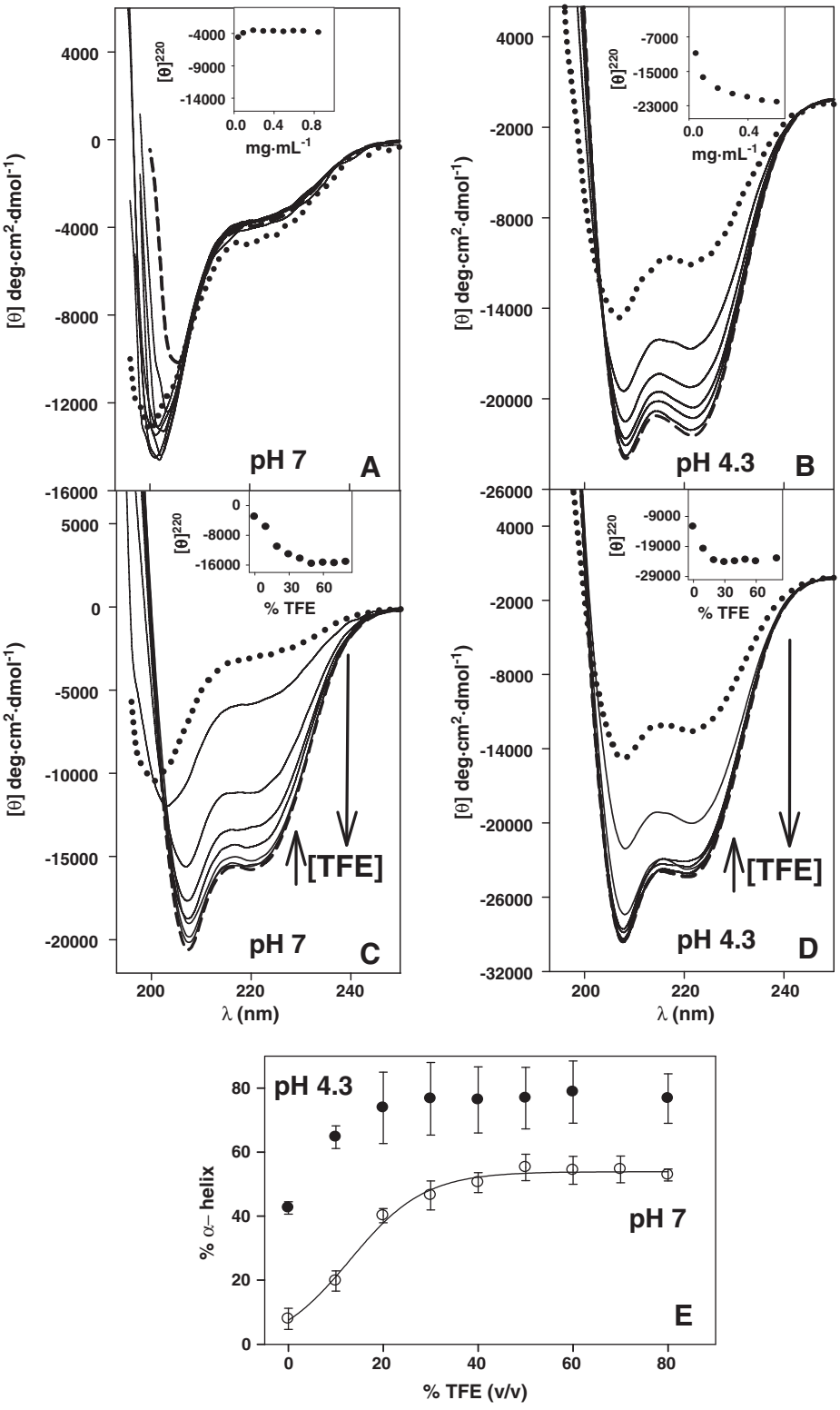

Fig. 7. Secondary structure of the peptide ^{60}W–E^{85} with and without TFE. A) CD spectra at peptide concentration between 0.05 mg mL^{-1} (dotted line) and 0.85 mg mL^{-1} (dashed line). Inset: Variation of the $[\theta]^{220}$ (same units) with peptide concentration. B) CD spectra of 0.05 mg mL^{-1} (dotted line) to 0.60 mg mL^{-1} (dashed line) at pH 4.3. Inset: Variation of $[\theta]^{220}$ with peptide concentration. C) CD spectra of 0.09 mg mL^{-1}peptide (dotted line) and with increasing amounts of TFE up to 80% (v/v, dashed line). Inset: Variation of $[\theta]^{220}$ with TFE concentration. D) Same as in C but at pH 4.3. E) Dependence of α-helix percent content on TFE concentration at pH 7 (void circles) and pH 4.3 (filled circles). Data at pH 7 were fitted to Eq. (2).

coiled coil such as syntaxin-1A, SNAP-25 or synaptobrevin-2, were unstructured in aqueous solution at any pH, ionic strength or peptide concentration and only adopted α-helical conformation in the presence of TFE [54]. Myosin-10, another 120-residue peptide predicted to form coiled coil, formed stable monomers even at concentrations in the mM range as deduced from CD, NMR and analytical ultracentrifugation [55].

The CD spectra of peptide ^{60}W–E^{85} at pH 4.3 in the range of 0.05–0.6 mg mL^{-1} (Fig. 7B) display the double minima at 208 and 220 nm characteristic of α-helical conformation, with both minima increasing their negative ellipticity as the peptide concentration increases. The variation of $[\theta]^{220}$ with peptide concentration (inset) is indicative of an oligomerization process taking place. It is known that the more stable the coiled coil, the lower the peptide concentration required to form the dimer. As the concentration of peptide is increased, the monomer-dimer equilibrium is likely shifted toward the formation of the coiled coil dimer, which increases the α-helical content of the peptide as it has been shown for other peptides in a pertinent example [56]. It may occur as in other example, the leucine zipper moiety of the GCN4 protein, that monomers are unstructured but adopt a α-helical conformation concomitant with oligomerization [57]. The CD analysis of our peptide at acidic pH, shows that the ratio $[\theta]^{220}/[\theta]^{208}$ varied from 0.75 to 0.94 as the peptide concentration increased from 0.05 to 0.60 mg mL^{-1} (not shown). Although the ratio is <1 at any concentration tested, approaching to 1 at the higher concentration is usually taken as indicative of peptide coiled coil formation. It is important to consider that the behavior of peptides does not necessarily match what is expected for proteins. The criteria used to establish that synthetic peptides form coiled coil are that their CD spectra show the double ellipticity minima at 208 and 220 nm with high negative ellipticities characteristics of a fully α-helix and that their ellipticity at 220 nm shows concentration dependence [58]. The relevance of middle acidic pH for a peptide to form oligomers has been found in other peptides and proteins. For example, the hemagglutinin of influenza virus forms a helical trimer that triggers membrane fusion only at acidic pH [59]. It has commonly been observed that coiled coils are more stable at low than at neutral pH, despite the loss of ion pairs by protonation of acidic residues at low pH. This phenomenon has been attributed to the finding that a protonated Glu at position **g** is intrinsically more stabilizing to the coiled coil by 0.65 kcal mol^{-1} over an ionized Glu interacting with Lys at 150 mM NaCl. This is likely due to both the higher helical propensity and the more hydrophobic character of Glu, which allows it to better pack at the dimer interface. Moreover, in the absence of a Lys at the dimer interface, the protonation of Glu results in a larger increase in coiled coil stability and does not depend on salt in the medium [60]. In this sense, a potential protonation at acidic pH of Glu in peptide ^{60}W–E^{85} would show an additional stabilizing effect since it would minimize unfavorable charge repulsions **g–g′**.

Different amounts of TFE were added to 0.09 mg mL^{-1} of peptide at pH 7 or 4.3 in order to generate solvent conditions known to support formation of helical peptide folding. The spectra acquired at pH 7 (Fig. 7C) clearly show that, under the influence of TFE, there is a propensity to switch from random coil (no TFE, dotted line) to α-helical conformation (80% TFE, dashed line). The maximal negative ellipticity at 220 nm is reached at about 50% TFE as indicated by the plateau (Fig. 7C, inset). The addition of increasing concentrations of TFE to the peptide at pH 4.3 (Fig. 7D), increases dramatically the negative ellipticity, with $[\theta]^{220}$ reaching plateau at ~20% TFE (inset) as the peptide already displays a strong α-helical conformation in the absence of TFE.

Regarding the α-helical content of the peptide vs TFE concentration, Fig. 7E shows that the α-helix in the absence of TFE, which practically does not exist at neutral pH (~7%), increases gradually with TFE until stabilization at ~40% TFE. The fitting of the data to Eq. (2) gave a midpoint of 12.9 ± 2.6% TFE and a plateau at 55.4 ± 7.3% TFE, which indicates the maximum helicity the peptide can reach in the presence of TFE at this pH. Shifting pH to 4.3, an initial 42.6 ± 1.9% α-helix without TFE increased to ~78% upon addition of TFE higher than 20% (v/v). The fitting of the data at acidic pH to Eq. (2) was not allowed since the Durbin–Watson Statistic and the Constant Variance Test of the data were not passed. These results indicate that the maximum helicity the peptide can reach with TFE at pH 7 is far less than the helicity reached at acidic pH once Glu residues should be mostly protonated.

3.8. Sedimentation analysis of peptide ^{60}W–E^{85}

The analysis by sedimentation velocity (SV) of the hydrodynamic properties of small peptides is difficult, but we have used it to complement the information we can extract from the most appropriated analysis by sedimentation equilibrium (SE). SV experiments were carried out with 0.55 mg mL^{-1} peptide and the c(s) profiles at pH 7 and pH 4.3 and 20 °C are plotted in Fig. 8A and B respectively. The profile at pH 7 (Fig. 8A) is consistent with the existence of a single homogeneous species (59.5% of the loaded peptide mass), with s = 0.53 S, a Stokes Radius of 1.33 nm and $s_{20,w}$ = 0.55 S (Mr ~ 3 kDa) with best frictional ratio f/f0 = 1.395, which indicates that the species is slightly elongated: a/b (oblate) = 5.29, a/b (prolate) = 4.91. This species is compatible with a monomer of peptide ^{60}W–E^{85} (theoretical Mr = 2957 Da). When the SV experiment was carried out at pH 4.3, the corresponding sedimentation profile in Fig. 8B shows that the species accounting for 72.9% mass shows s = 1.672 S, a Stokes Radius of 1.97 nm and $s_{20,w}$ = 1.735 S (Mr ~14 kDa) with best frictional ratio f/f0 = 1.241 (the shape of the oligomer would approaches the sphere), a/b (oblate) = 1.97, a/b (prolate) = 2.91. This species is compatible with an oligomer.

Sedimentation equilibrium of 0.55 mg mL^{-1} peptide at pH 7 or pH 4.3 was carried out at 20 °C and 28,000 rpm and the obtained absorbance gradients were converted to the corresponding weight-average molecular weight (Mw,a). The buoyant molar mass (the molar mass of solute reduced by the molar mass of the solvent displaced by the solute) was 749 ± 2 Da and the calculated averaged molecular weight was 2826 at pH 7 which corresponds to the molecular mass of the monomeric peptide (2957 Da) and agrees well with the apparent molecular mass estimated from SV analysis (~3 kDa). The experimental data are represented in Fig. 8C as symbols and the line is the fitting of data to a single species. The residuals (difference between values predicted by the model and the values actually observed) were plotted against radius to asses the goodness of the fit. The random distribution of the residuals indicates that the data fit well to an ideal single-species model, therefore confirming that the peptide is monomeric. The low root mean squares (RMS) deviation, $3.3 \cdot 10^{-3}$, also points to the goodness of the fit. Attempts to use a model with oligomerization equilibrium did not improve the quality of the fitting.

The SE analysis of the peptide was also carried out at pH 4.3 and the experimental data could not be fitted to a single species since they formed a V up and down of the solid line representing a single species in the residuals distribution (Fig. 8D, RMS deviation = $7.7 \cdot 10^{-3}$). It points to a typical case of multiple polydisperse association. The best fit of the data was obtained to the Monomer–Nmer–Mmer model being N = 6 and M = 4 (the fitting line and the residuals are not shown; RMS deviation = $3.1 \cdot 10^{-3}$). The buoyant molar mass was 3892 ± 28 Da and the calculated weight-averaged molecular weight was 14692, close to the apparent molecular mass obtained in SV analysis (~14 kDa) at acid pH. Thus, SE data point to the peptide associating into tetramers and hexamers at acidic pH whereas it remains monomeric at neutral pH. This behavior, together with the CD data presented above, suggests that secondary structure stabilization and oligomerization occur together and must be concerted processes.

4. Discussion

The conformation of the N-terminal propeptide (SP-B_N) of the precursor (proSP-B) of surfactant protein B (SP-B) suffers a notable change around pH 4.3, revealed by the inversion of the ellipticity minima at 208 and 220 nm of its CD spectrum. This inversion, with the concomitant change of the ratio $[\theta]^{220}/[\theta]^{208}$ from <1 (pH 7) to >1 (pH 4.3), suggests that SP-B_N forms a coiled coil structure at acidic pH. The apparent pK of the group whose protonation triggers the structural change is 4.8 ± 0.06, close to the one triggering changes in the fluorescence properties of the protein, indicating that the same group (likely a carboxyl) is

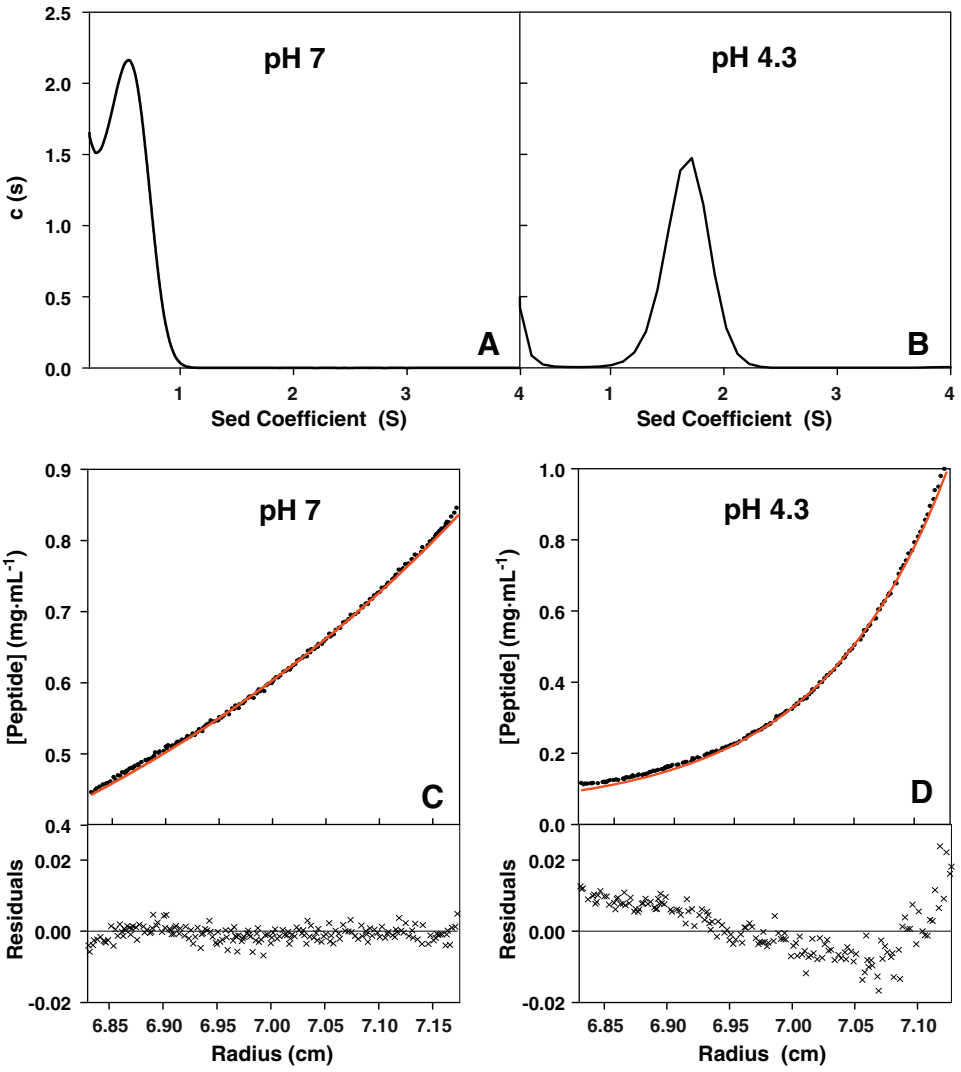

Fig. 8. Sedimentation velocity and sedimentation equilibrium analysis of the peptide $^{60}W–E^{85}$. Sedimentation coefficient distribution of the peptide in 5 mM AMT buffer, 150 mM NaCl pH 7 (A) and pH 4.3 (B). Sedimentation equilibrium gradients of the peptide in the same buffer either at pH 7 (C) or pH 4.3 (D). In C and E the symbols represent the experimental data and the solid line is the fit of the experimental data to a single ideal species. The residual distribution as a function of the sedimentation distance is inset in the bottom of both plots and corresponds to the difference between the experimental data and the fitted data for each point.

responsible for changes in both, the secondary and tertiary structure of SP-B_N upon acidification of the medium. The dependence of the $[\theta]^{208}$ on protein concentration at acidic but not at neutral pH reinforces the hypothesis of coiled coil formation at acidic pH. Additional evidence was obtained from the secondary structure of SP-B_N in the presence of a halogenated alcohol such as TFE as cosolvent at acidic pH. TFE concentrations above 40% (v/v) promoted α-helix and disassembled coiled coil structures, reverting the $[\theta]^{220}/[\theta]^{208}$ ratio to less than 1. One could argue that spectral changes such as those registered systematically in our experiments could be also due to other types of conformational changes, but their association with the acquisition of a coiled coil structure has been confirmed by different techniques, both in the whole SP-B_N protein and in the synthetic peptide designed to mimic the predicted coiled coil segment of proSP-B_N. Coiled coil structures are responsible of oligomerization processes and as we have gel filtration and DLS results (see supplementary data) pointing to the existence of SP-B_N oligomers, the association state of SP-B_N was analyzed by velocity sedimentation. A population of species compatibles with dimers, tetramers and hexamers (coexisting with species displaying higher molecular mass) were observed at neutral pH. The population was enriched in the species compatible with the tetramer upon pH acidification, pointing to this species as the one holding coiled coil structure. That is, two SP-B_N dimers would interact forming a coiled coil structure at pH 4.3. It is possible that the tetramers existing at pH 7 may also hold the coiled coil structure but they are not the predominant species at neutral pH (as they are at pH 4.3).

The propensity of SP-B_N to form coiled coil structure is predicted by several programs, which identify a patch of residues close to the N-terminal end of the SAPB domain as potentially responsible. The different experimental evidences together with the prediction studies support that the segment $^{65}A–E^{85}$ dimerizes by forming an antiparallel coiled coil, triggered by the protonation of Glu residues (E^{71} and E^{85}) at acidic pH that would eliminate charge repulsion and would stabilize the coiled coil. Complementary results of sedimentation velocity at very low ionic strength (no salt added), point to SP-B_N dissociating into monomers (not shown) suggesting, together with the pH results of the present work, that electrostatic repulsion affects significantly the energy of self-association. A 26-residue synthetic peptide encompassing the sequence predicted to form coiled coil become in fact structured upon pH acidification, while it transits

from a monomeric into an oligomeric state, as detected by sedimentation velocity and sedimentation equilibrium analysis.

On the other hand, the prediction of ordered parallel β-aggregation in a 6-residues patch overlapping with the coiled coil predicted region, together with the binding of Thioflavin T to SP-B_N at acidic pH and 10–30% TFE suggests the existence of a region in the SAPB domain of SP-B_N with structural plasticity. Since SP-B_N is thought to act as chaperone of mature SP-B [9] while its SAPB domain shows microbicide properties [13], this conformational flexibility might help to define particular functions under different environmental conditions.

The acidic pH-triggered concerted association of the SP-B_N domain of proSP-B, *via* formation of a coiled-coil motif, is highly relevant for at least two processes. It has been demonstrated that the proteolitic maturation of proSP-B and the assembly of mature pulmonary surfactant protein SP-B into surfactant lipid–protein complexes, as it occurs in type II pneumocytes, is tightly coupled to pH acidification along the pathway of lamellar body biogenesis [61]. Likewise, it has been proposed that the SP-B_N domain is necessary and sufficient to facilitate folding and proper targeting of the mature SP-B sequence into an operative surfactant [7]. In this sense, the SP-B_N module has been proposed to act as an intramolecular chaperone, in charge of protecting the extremely hydrophobic sequence of mature SP-B from inappropriate interactions until the precise moment in which it has to integrate into surfactant membranes [9]. Proteolytic processing of proSP-B by specific enzymes, including napsin A and several cathepsins depends also on acidic pH [62,63]. Previous data suggested that the saposin modules of proSP-B could exhibit interaction with membranes early after their synthesis, still at neutral pH [64]. This superficial orientation would impose a defined geometry, which, upon acidification, might induce a coiled-coil-mediated orientated oligomerization to conformations that would expose the most hydrophobic module of the precursor to a deeper penetration into surfactant membranes. Therefore, pH-dependent oligomerization of the SP-B_N domain, *via* coiled coil formation, might be the critical structural feature triggering the exposure of the hydrophobic SP-B module in proSP-B, its insertion into the hydrophobic core of membranes, and the parallel unmasking of proSP-B cleavage sites. The pH at which such conformational change is triggered, around 4.8, is consistent with the level of pH acidification expected along the pathway of surfactant biogenesis in pneumocytes, through multivesicular and lamellar bodies [61,65]. On the other hand, once maturation of proSP-B and surfactant biogenesis and secretion has been completed, the SAPB domain of SP-B_N has been detected as an independent protein in the alveolar spaces, with a conspicuous microbicidal activity which is also critically dependent on acidic pH [13]. It has been proposed that the antibiotic properties of SP-B_N could be important to kill bacteria at the endosomal compartments of alveolar macrophages, once they have been phagocyted. The coiled coil-related conformational change described here could be part of the pH-dependent capacitation of SP-B_N into the competent structure that has the ability to compromise the viability of pathogens, likely through permeation of their membranes.

Conformational changes and oligomerization involving coiled-coil formation could be a general feature of all the proteins containing the saposin-like fold. Apart of our data obtained from the study of SP-B_N, the three-dimensional structure of saposin B as determined by crystallization and X-ray diffraction, also revealed coiled coil-driven dimerization, to form an structure that gains the ability to bind and solubilize a phospholipid molecule [14]. We have recently proposed a model in which dimerization and higher order oligomerization could be essential for the action mechanism of saposins, either to promote mobilization of surface active lipids in surfactant or to permeabilize membranes by cytolysines [66]. Our results suggest that the self-associating interface in the dimer, or in the higher order oligomers, could be defined by a coiled-coil motif, which in some of the saposins, such as SP-B_N, could also require a proper electrostatic tuning *via* pH, which would trigger self-association in defined physiological contexts. Self-association *via* coiled-coil would ensure specificity, robustness and a proper geometry to form a high order assembly that might be competent to resist demanding mechanical stress, such as those at the high pressures imposed by highly compressed respiratory surface films at the end of expiration.

A pertinent question would be whether the oligomers formed by SP-B_N at acidic pH could define the geometry of proSP-B as a whole and its processing to render the active complex in pulmonary surfactant, or whether these oligomers would define the required structure to permeabilize membranes and therefore the ability of SP-B_N to exhibit antibiotic properties. In other words, would SP-B_N tetramers, or hexamers, be real intermediates in the assembly of functionally competent surface- or membrane-active protein assemblies? This is an open question that will require further investigation. The coiled-coil motif revealed in the present study likely ensures a well-defined pH-dependent assembly, which, under the most relevant physiological conditions, will also include modulation by interaction with phospholipid membranes. All the saposins share the ability to interact with phospholipid bilayers, *via* amphipathic helical segments that associate more or less deeply into the headgroup region of membranes [67]. We have proposed that the interaction of saposins with the membrane surface imposes orientated protein–protein interactions that are crucial to define functional oligomerization [66]. We speculate that coiled-coil supramolecular oligomerization could be modulated in the presence of membranes, leading to a geometry that could be only partly acquired in their absence. In the present work, we detect formation by SP-B_N of tetramers and hexamers. The SAPB domain of SP-B_N was shown previously to have membrane-interaction properties at neutral pH, transiting to forms with deeper membrane penetration at acidic pH [13]. It is conceivable that the orientation of the propeptide upon interaction at the surface of membranes imposes restrictions that facilitate the acquisition of the functional oligomeric structure, whatever it is. Future studies will extend the conformational characterization of SP-B_N and the coiled-coil motif, at neutral and acidic pH, in the context of the negatively-charged membranes typical of pulmonary surfactant.

Acknowledgements

The authors are indebted to Dr. Carlos Alfonso, from Centro de Investigaciones Biologicas of the Spanish Research Council (CSIC), for their technical assistance to carry out the analytical centrifugation experiments. This research has been funded by grants from the Spanish Ministry of Economy and Competitivity (BIO2012-30733, CSD2007-0010), the Regional Government of Madrid (S2009MAT-1507) and Complutense University (910483-1115).

Appendix A. Supplementary data

Supplementary data to this article can be found online at http://dx.doi.org/10.1016/j.bbamem.2014.03.016.

References

[1] F.H.C. Crick, Is alpha-keratin a coiled coil? Nature 170 (1952) 882–883.
[2] R. Straussman, A. Ben-Ya'acov, D.N. Woolfson, Kinking the coiled coil-negatively charged residues of the coiled coil interface, J. Mol. Biol. 366 (2007) 1232–1242.
[3] M.R. Hicks, D.V. Holberton, C. Kowalczyk, D.N. Woolfson, Coiled-coil assembly by peptides with non-heptad sequence motifs, Fold. Des. 2 (1997) 149–158.
[4] B. Berger, D.B. Wilson, E. Wolf, T. Tonchev, M. Mila, P.S. Kim, Predicting coiled coils by use of pairwise residue correlation, Proc. Natl. Acad. Sci. 92 (1995) 8259–8263.
[5] D.A. Parry, Coiled-coils in α-helix-containing proteins: analysis of the residue types within the heptad repeat and the use of these data in the prediction of coiled-coils in other proteins, Biosci. Rep. 2 (1982) 1017–1024.
[6] T.E. Weaver, J.J. Conkright, Function of surfactant proteins B and C, Annu. Rev. Physiol. 63 (2001) 555–578.
[7] S. Lin, H.T. Akinbi, J.S. Breslin, T.E. Weaver, Structural requirements for targeting of surfactant protein B (SP-B) to secretory granules in vitro and in vivo, J. Biol. Chem. 271 (1996) 19689–19695.
[8] F. Brasch, G. Johnen, A. Winn-Brasch, S.H. Guttentag, A. Schmiedl, N. Kapp, Y. Suzuki, K.M. Muller, J. Richter, S. Hawgood, M. Ochs, Surfactant protein B in type II pneumocytes and intra-alveolar surfactant forms of human lungs, Am. J. Respir. Cell Mol. Biol. 30 (2004) 449–458.

[9] S. Lin, K.S. Phillips, M.R. Wilder, T.E. Weaver, Structural requirements for intracellular transport of pulmonary surfactant protein B (SP-B), Biochim. Biophys. Acta 1312 (1996) 177–185.
[10] A. Palacios, B. González, S. Alonso, J. Pérez-Gil, P. Estrada, Production of a recombinant form of the propeptide NH_2-terminal of the precursor of pulmonary surfactant protein B, Enzym. Microb. Technol. 40 (2006) 85–92.
[11] A. Bañares-Hidalgo, A. Bolaños-Gutierrez, F. Gil, E.J. Cabré, J. Pérez-Gil, P. Estrada, Self-aggregation of a recombinant form of the propeptide NH2-terminal of the precursor of pulmonary surfactant protein SP-B: a conformational study, J. Ind. Microbiol. Biotechnol. 35 (2008) 1367–1376.
[12] L. Patthy, Homology of the precursor of pulmonary surfactant-associated protein SP-B with prosaposin and sulfated glycoprotein, J. Biol. Chem. 266 (1991) 6035–6037.
[13] L. Yang, J. Johansson, R. Ridsdale, H. Willander, M. Fitzen, H.T. Akinbi, T.E. Weaver, Surfactant protein B propeptide contains a saposin-like protein domain with antimicrobial activity at low pH, J. Immunol. 12 (2010) 975–983.
[14] V.E. Ahn, K.F. Faull, J.P. Whitelegge, A.L. Fluharty, G.G. Privé, Crystal structure of Saposin B reveals a dimeric shell for lipid binding, Proc. Natl. Acad. Sci. 100 (2003) 38–43.
[15] L.A. Kelley, M.J.E. Sternberg, Protein structure prediction on the web: a case study using the Phyre server, Nat. Protoc. 4 (2009) 363–371.
[16] M. Gustaffson, J. Thyberg, J. Näslund, E. Eliasson, J. Johansson, Amyloid fibril formation by pulmonary surfactant protein C, FEBS Lett. 464 (1999) 138–142.
[17] A. Trovato, F. Seno, S.C. Tosatto, The PASTA server for protein aggregation prediction, Protein Eng. Des. Sel. 20 (2007) 521–523.
[18] C.C. Mahrenholz, I.G. Abfalter, U. Bodenhofer, R. Volkmer, S. Hochreiter, Complex networks govern coiled coil oligomerization—predicting and profiling by means of a machine learning approach, Mol. Cell. Proteomics 10 (2011) (M110.004994).
[19] A. Gonzalez-Horta, D. Andreu, M.R. Morrow, J. Pérez-Gil, Effects of palmitoylation on dynamics and phospholipid-bilayer-perturbing properties of the N-terminal segment of pulmonary surfactant protein SP-C as shown by 2H-NMR, Biophys. J. 95 (2008) 2308–2317.
[20] N. Sreerama, R.W. Woody, Estimation of protein secondary structure from circular dichroism spectra: comparison of CONTIN, SELCON, and CDSSTR methods with an expanded reference set, Anal. Biochem. 287 (2000) 252–260.
[21] T.M. Laue, B.D. Shah, T.M. Ridgeway, S.L. Pelletier, Computer-aided interpretation of analytical sedimentation data for proteins, in: S.E. Harding, A. Rowe, J.C. Horton (Eds.), Analytical Ultracentrifugation in Biochemistry and Polymer Sciences, Royal Soc. Chem., Cambridge, 1992, pp. 90–125.
[22] http://au.expasy.org/cgi-bin/protparam .
[23] http://www.biotech.uconn.edu/auf .
[24] J. Garnier, D.J. Osguthorpe, B. Robson, Analysis of the accuracy and implications of simple methods for predicting the secondary structure of globular proteins, J. Mol. Biol. 120 (1978) 97–120.
[25] D.T. Jones, Protein secondary structure prediction based on position-specific scoring matrices, J. Mol. Biol. 292 (1999) 195–205.
[26] A. Lupas, M. Van Dyke, J. Stock, Predicting coiled coils from protein sequences, Science 252 (1991) 1162–1164.
[27] A. Lupas, S. Müller, K. Goldie, A.M. Engel, A. Engel, W. Baumeister, Model structure of the Ompα rod, a parallel four-stranded coiled coil from the hyperthermophilic eubacterium *Thermotoga maritime*, J. Mol. Biol. 248 (1995) 180–189.
[28] V.A. Fischetti, G.M. Landau, J.P. Schmidt, P. Sellers, Identifying periodic occurrence of a template with applications to protein structure, Inform. Proc. Lett. 45 (1993) 11–18.
[29] http://emboss.bioinformatics.nl .
[30] E. Wolf, P.S. Kim, B. Berger, Multicoils: a program for predicting two- and three-stranded coiled coils, Prot. Sci. 6 (1997) 1179–1189.
[31] http://agadir.crg.es .
[32] S.Y.M. Lau, A.K. Taneja, R.S. Hodges, Effect of chain length on the stabilization and formation of two-stranded α-helical coiled-coils, J. Biol. Chem. 259 (1984) 13253–13261.
[33] W.D. Anderson, A.L. Fink, L.J. Perry, R. Wetzel, Effect of an engineered disulfide bond on the folding of T4 lysozyme at low temperatures, Biochemistry 29 (1990) 3331–3337.
[34] P.P. De Laureto, D. Vinante, E. Scaramella, E. Frare, A. Fontana, Stepwise proteolytic removal of the β subdomain in α-lactalbumin. The protein remains folded and can form the molten globule in acid solution, Eur. J. Biochem. 268 (2001) 4324–4333.
[35] Y. Chen, M.D. Barkley, Towards understanding tryptophan fluorescence in proteins, Biochemistry 37 (1998) 9976–9982.
[36] N.E. Zhou, C.M. Kay, R.S. Hodges, Synthetic model proteins, Positional effects of interchain hydrophobic interactions on stability of two-stranded α-helical coiled-coils, J. Biol. Chem. 267 (1992) 2664–2670.
[37] G. Plakoutsi, F. Bemporad, M. Calamai, N. Taddei, C.M. Dobson, F. Chiti, Evidence for a mechanism of amyloid formation involving molecular reorganisation within native-like precursor aggregates, J. Mol. Biol. 351 (2005) 910–922.
[38] N. Sreerama, S.Y. Venyaminov, R.W. Woody, Estimation of the number of α-helical and β-strand segments in proteins using circular dichroism spectroscopy, Protein Sci. 8 (1999) 370–380.
[39] J.S. Orlando, D. Ornelles, An arginine-faced amphipatic alpha helix is required for adenovirus type 5 E4orf6 protein function, J. Virol. 73 (1999) 4600–4610.
[40] A. Cammers-Goodwin, T.J. Allen, S.L. Oslick, K.F. McClure, J.H. Lee, D.S. Kemp, Mechanism of stabilization of helical conformations of polypeptides by water containing trifluoroethanol, J. Am. Chem. Soc. 118 (1996) 3082–3090.
[41] H. Reirsen, A.R. Rees, Trifluoroethanol may form a solvent matrix for assisted hydrophobic interactions between peptide side chains, Protein Eng. 13 (2000) 739–743.
[42] K. Yamaguchi, H. Naiki, Y. Goto, Mechanism by which the amyloid-like fibrils of a β_2-microglobulin fragment are induced by fluorine-substituted alcohols, J. Mol. Biol. 363 (2006) 279–288.
[43] D. Sambasivan, C.W. Liu, M. Jayaraman, E.J.P. Malar, J. Rajadas, Aggregation and conformational studies on a pentapeptide derivative, Biochim. Biophys. Acta 1784 (2008) 1659–1667.
[44] H. LeVine, Thioflavin T interaction with synthetic Alzheimer's disease β-amyloid peptides: detection of amyloid aggregation in solution, Protein Sci. 2 (1993) 404–410.
[45] S. Srisailam, T.S.K. Kumar, D. Rajalingam, K.M. Kathir, H.S. Sheu, F.J. Jan, Amyloid-like fibril formation in an all beta-barrel protein partially structured intermediate state(s) is a precursor for fibril formation, J. Biol. Chem. 278 (2003) 17701–17709.
[46] J.H. Brown, C. Cohen, D.A. Parry, Heptad breaks in α-helical coiled coils: stutters and stammers, Proteins 26 (1996) 134–145.
[47] M.O. Steinmetz, I. Jelesarov, W.M. Matousek, S. Honnappa, W. Jahnke, J.H. Missimer, S. Frank, A.T. Alexandrescu, R.A. Kammerer, Molecular basis of coiled-coil formation, Proc. Natl. Acad. Sci. 104 (2007) 7062–7067.
[48] K.M. Gernert, M.C. Surles, T.H. Labean, J.S. Richardson, D.C. Richardson, The Alacoil: a very tight, antiparallel coiled-coil of helices, Protein Sci. 4 (1995) 2252–2260.
[49] J.R. Apgar, K.N. Gutwin, A.E. Keating, Predicting helix orientation for coiled-coil dimers, Proteins 72 (2008) 1048–1065.
[50] P.B. Harbury, T. Zhang, P.S. Kim, T. Alber, A switch between two-, three- and four-stranded coiled coils in GCN4 leucine zipper mutants, Science 262 (1993) 1401–1407.
[51] A.D. Parry, R.B.D. Fraser, J.M. Squire, Fifty years of coiled-coils and a-helical bundles: a close relationship between sequence and structure, J. Struct. Biol. 163 (2008) 258–269.
[52] M. Vila-Perelló, S. Tognon, A. Sánchez-Vallet, F. García-Olmedo, A. Molina, D. Andreu, A minimalist design approach to antimicrobial agents based on a Thionin template, J. Med. Chem. 49 (2006) 448–451.
[53] C.B. Karim, M.G. Paterlini, L.G. Reddy, G.W. Hunter, G. Barany, D.D. Thomas, Role of cysteine residues in structural stability and function of a transmembrane helix bundle, J. Biol. Chem. 276 (2001) 38814–38819.
[54] J.M. Cànaves, M. Montal, Assembly of a ternary complex by the predicted minimal coiled coil-forming domains of syntaxin, SNAP-25 and Synaptobrevin. A circular dichroism study, J. Biol. Chem. 273 (1998) 34214–34221.
[55] P.J. Knight, K. Thirumurugan, Y. Xu, F. Wang, A.P. Kalverda, W.F. Stafford, J.R. Sellers, M. Peckham, The predicted coiled-coil domain of myosin 10 forms a novel elongated domain that lengthens the head, J. Biol. Chem. 280 (2005) 34702–34708.
[56] B.Y. Zhu, N.E. Zhou, C.M. Kay, R.S. Hodges, Packing and hydrophobicity effects on protein folding and stability: effects of β-branched amino acids, valine and isoleucine, on the formation and stability of two-stranded α-helical coiled coils/leucine zippers, Prot. Sci. 2 (1993) 383–394.
[57] N. Liu, G. Caderas, B. Gutte, R.M. Thomas, An artificial HIV enhancer-binding peptide is dimerized by the addition of a leucine zipper, Eur. Biophys. J. 25 (1997) 399–403.
[58] J. Liu, Q. Zheng, Y. Deng, C.S. Cheng, N.R. Kallenbach, M. Lu, A seven-helix coiled coil, Proc. Natl. Acad. Sci. U. S. A. 103 (2006) 15457–15462.
[59] C.M. Carr, P.S. Kim, A spring-loaded mechanism for the conformational change of influenza hemagglutinin, Cell 73 (1993) 823–832.
[60] W.D. Kohn, C.M. Kay, R.S. Hodges, Salt effects on protein stability: two-stranded-helical coiled-coils containing inter- or intrahelical ion pairs, J. Mol. Biol. 267 (1997) 1039–1052.
[61] W.F. Voorhout, T. Veenendaal, H.P. Haagsman, A.J. Verkleij, J.A. Van Golde, H.J. Geuze, Intracellular processing of pulmonary surfactant protein B in an endosomal/lysosomal compartment, Am. J. Physiol. 263 (1992) 479–486.
[62] F. Brasch, M. Ochs, T. Kahne, S. Guttentag, V. Schauer-Vukasinovic, M. Derrick, G. Johnen, N. Kapp, K.M. Muller, J. Richter, T. Giller, S. Hawgood, F. Buhling, Involvement of napsin A in the C- and N-terminal processing of surfactant protein B in type-II pneumocytes of the human lung, J. Biol. Chem. 278 (2003) 49006–490014.
[63] T. Ueno, S. Linder, C.L. Na, W.R. Rice, J. Johansson, T.E. Weaver, Processing of pulmonary surfactant protein B by napsin and cathepsin H, J. Biol. Chem. 279 (2004) 1678–1684.
[64] A.G. Serrano, E.J. Cabré, J.M. Oviedo, A. Cruz, B. Gonzalez, A. Palacios, P. Estrada, J. Perez-Gil, Production in *Escherichia coli* of a recombinant C-terminal truncated precursor of surfactant protein B (proSP-$B_{\Delta C}$). Structure and interaction with lipid interfaces, Biochim. Biophys. Acta 1758 (2006) 1621–1632.
[65] A. Korimilli, L.W. Gonzales, S.H. Guttentag, Intracellular localization of processing events in human surfactant protein B biosynthesis, J. Biol. Chem. 275 (2000) 8672–8679.
[66] B. Olmeda, B. Garcia-Alvarez, J. Pérez-Gil, Structure–function correlations of pulmonary surfactant protein SP-B and the saposin-like family of proteins, Eur. Biophys. J. 42 (2013) 209–222.
[67] H. Bruhn, A short guided tour through functional and structural features of saposin-like proteins, Biochem. J. 389 (2005) 249–257.